Topology effects on nonaffine behavior of semiflexible fiber networks

H. Hatami-Marbini* and V. Shriyan

Department of Mechanical & Industrial Engineering, University of Illinois at Chicago, Chicago, Illinois 60607, USA

(Received 12 July 2017; published 20 December 2017)

Filamentous semiflexible networks define the mechanical and physical properties of many materials such as cytoskeleton. In the absence of a distinct unit cell, the Mikado fiber network model is commonly used algorithm for representing the microstructure of these networks in numerical models. Nevertheless, certain types of filamentous structures such as collagenous tissues, at early stages of their development, are assembled by growth of individual fibers from random nucleation sites. In this work, we develop a computational model to investigate the mechanical response of such networks by characterizing their nonaffine behavior. We show that the deformation of these networks is nonaffine at all length scales. Furthermore, similar to Mikado networks, the degree of nonaffinity in these structures decreases with increasing the probing length scale, the network fiber density, and/or the bending stiffness of constituting filaments. Nevertheless, despite the lower coordination number of these networks, their deformation field is more affine than that of the Mikado networks with the same fiber density and fiber mechanical properties.

DOI: 10.1103/PhysRevE.96.062502

I. INTRODUCTION

A network of random semiflexible filaments constitutes the primary building block of different biological and nonbiological materials [1–3]. For instance, paper, felt, and similar nonwoven materials are composed of a network of entangled filaments [4,5]. Furthermore, properties of many soft tissues are governed by a complex and intertwined network of collagen and elastin fibers. Cytoskeleton is a network of interlinking fibers, which helps cells maintain their shape and perform important activities such as migration and division [6–8]. In semiflexible random fiber networks, the bending stiffness of filaments is large enough to prevent them from folding into a random coil because of their configurational entropy. This notable feature leads to unique mechanical properties, not seen in flexible polymer networks, such as strain stiffening and negative normal stress [9–11].

Unlike rubbers and flexible networks, affine models [12] cannot accurately describe the deformation of semiflexible networks. Affine models assume that filaments stretch and rotate as if they are attached to a homogenous continuum and follow the applied macroscopic deformation. However, it is well known that the behavior of random semiflexible filamentous networks, like many other disordered structures, is nonaffine; i.e., there exist fluctuations from affine displacement. Because of these fluctuations, the overall response of these systems is much softer than what the affine approximation gives. In recent decades, extensive computational efforts have been devoted to better understand the nonaffine response of semiflexible fiber networks and to determine conditions under which an affine model may be used to predict their mechanical fields [13–19].

Nonaffine deformation of disordered discrete systems can be characterized by nonaffine correlation functions, commonly referred to as nonaffinity measures [20]. There are several nonaffinity measures in the literature. For example, Langer and Liu [21] and Tanguy *et al.* [22] characterized the nonaffine response of foams and polydisperse Lennard-Jones beads by measuring the mean squared average of displacement fluctuations. This measure has also been used to characterize the nonaffine response of random filamentous networks [15,23]. Despite the simplicity of this measure in implementation and formulation, it is not capable of characterizing the effects of the probing length scale on nonaffine behavior of random structures. In order to circumvent this disadvantage, Head *et al.* [15] used the scalar measure $\langle(\theta - \theta^{\mathrm{af}})^2\rangle_r$ which calculates the change of angle θ, made by a vector connecting two arbitrary cross-links at a distance r, due to the applied far field and its corresponding affine estimate, θ^{af}. Furthermore, Hatami-Marbini and Picu [16] introduced a strain-based nonaffinity measure based on the local displacement gradient field at various probing length scales. The above studies have shown that the degree of nonaffine response of random semiflexible fiber networks, when subjected to small far-field deformation, primarily depends on their fiber density and flexibility of their constituting filaments. Other important conclusions regarding the behavior of filamentous networks have been drawn from the above and similar studies [1–3]. However, the network microstructure has been represented by a two-dimensional (2D) Mikado model in most of these studies.

Mikado networks are generated by depositing filaments of constant length with random orientations into a square domain [14–16]. Two-dimensional fiber networks can alternatively be constructed by growing filaments from randomly positioned seed points in a square domain and stopping their growth when they reach each other or the domain boundary [24]. Despite the popularity of the Mikado model, this alternative model seems more appropriate for representing certain types of filamentous structures such as collagenous tissues. These biological structures, especially at their initial stages of development, are assembled by growth of their individual fibers from nucleation sites [24–26]. The main objective of this work is to investigate whether there exist any notable differences in the mechanical response of 2D Mikado polymer networks from that of 2D models created by this alternative approach.

The above random networks have different coordination numbers. The coordination number z of a polymer network significantly influences its mechanical properties and is defined

*hatami@uic.edu

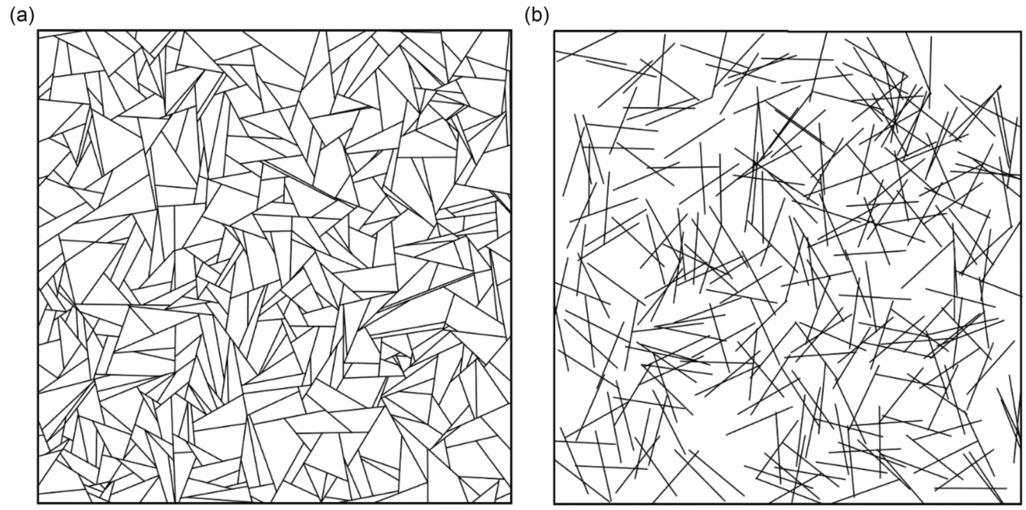

FIG. 1. Example of random fiber networks generated by different algortihms: (a) Type I networks are constructured by growing straight lines from randomly positioned seed points. (b) Type II networks (Mikado networks) are generated by depositing straight lines in a domain. There are three line segments at each intersection point of a type I network and four line segments at each cross-link of a type II (Mikado) network.

as the number of neighboring fibers at cross-links. In 2D networks, which are composed of filaments with no bending stiffness, the required coordination number for mechanical stability is at least 4 (Maxwell central-force isostatic threshold). Mikado networks have a coordination number of $z = 4$ because no more than two fibers cross exactly at the same location. However, $z = 3$ for the networks that are generated using the alternative algorithm. Thus, these networks are below Maxwell central-force isostatic threshold and are expected to show more nonaffine deformation.

Here, we develop a computational model for the mechanical response of 2D fiber networks generated using Mikado and fiber growing algorithms. We use a scalar and a strain-based nonaffinity measure to characterize the effects of network microstructure on displacement and strain distribution at different length scales. Although two network types exhibit qualitatively similar behavior, we observe significant differences. In both types of networks, we find that strain-based nonaffinity components decay with probing length scale following a power law. Moreover, we show that the nonaffinity is inversely proportional to the network fiber density. Nevertheless, we observe that the nonaffinity is unexpectedly more pronounced in Mikado networks, which have a larger coordination number. The density and energy distribution inside both types of random fiber networks are studied to explain and provide insight into this observation.

II. MODEL

The networks are constructed by growing straight cylindrical fibers with radius R from randomly distributed nucleation sites in a domain. Specifically, following a uniform deposition of seed points into a square domain of size W, straight filaments are grown with a constant growth rate from each point. The growth of a filament stops when it reaches the edges of the square domain or if it reaches another filament. A rigid permanent cross-link is considered between intersecting filaments [16]. We will refer to these networks as type I networks in this work. A representative network is shown in Fig. 1(a).

We also create Mikado fiber networks by depositing straight cylindrical filaments of constant length L_0 in a square domain [16]. The location of the center and orientation of fibers are uniformly distributed over allowable ranges and rigid connections are assumed when two fibers cross. We refer to Mikado networks as type II networks in the present study. Unlike type I networks, dangling ends will be created in these networks. The dangling ends will be ignored in the analysis since they do not have any contribution to the total energy of the structure. Another important difference is that, unlike type I networks, which always form a percolated structure, a critical fiber density is required for type II networks to acquire rigidity [14,15]. Figure 1(b) shows a typical type II fiber network.

Both network types are loaded by a displacement-imposed boundary condition; i.e., the displacements are prescribed on the boundaries of the simulation domain [15,16]. Only small strain uniaxial loadings are considered and the energy minimization technique is used to obtain the solution. The mechanical response of fibers is determined by a bending modulus κ and a stretching modulus μ. The ratio of the bending and stretching modulus of the fibers represents their flexibility and is denoted by $l_b = \sqrt{\kappa/\mu}$. The total energy of the system is given by the sum of the Hamiltonian of all individual filaments, i.e.,

$$H_i = \frac{1}{2}\int \mu\left(\frac{\partial l}{\partial s}\right)^2 + \kappa\left(\frac{\partial \phi}{\partial s}\right)^2 ds, \quad i = 1\cdots N_f, \qquad (1)$$

where s is the arc length of a filament, $\partial l/\partial s$ is its extensional deformation, and ϕ is the angle of the tangent of the filament. The first and second terms in Eq. (1) represent the energy stored in a filament due to stretching and bending deformation, respectively.

Once the solution of the system is obtained, the amount of nonaffinity in the behavior of the fiber networks is characterized using a scalar nonaffinity measure γ and a length-scale-dependent nonaffinity measure H_i [15,16]. The scalar nonaffinity measure γ is easy to calculate and measure in experiments. It is given by

$$\gamma = \frac{1}{\varepsilon_{\text{applied}}^2 W^2} \langle (\Delta \mathbf{u})^2 \rangle, \tag{2}$$

where $\varepsilon_{\text{applied}}$ is the applied uniform far-field strain, $\Delta \mathbf{u} = \mathbf{u}_i - \mathbf{u}_i^{\text{affine}}$, $\mathbf{u}_{\text{i}}$ is displacement vector of the ith cross-link, superscript "*affine*" denotes the affine estimate of the displacement vector, and angle brackets represent averaging $\Delta \mathbf{u}$ over all cross-linking points in the fiber network. The length-scale-dependent strain-based nonaffinity measure $H_i(r)$ is defined as

$$H_i(r) = \frac{1}{\varepsilon_{\text{applied}}^2} \left\langle \left(\varepsilon_i - \varepsilon_i^{\text{affine}} \right)^2 \right\rangle_r, \quad i = 1,2,3, \tag{3}$$

where, ε_1, ε_2, and ε_3 are the respective uniaxial, normal, and shear strains, and r is the probing length scale. A method similar to tensometry is used to obtain the strain components ε_i at different length scales. Briefly, the strain is calculated on scale r by selecting triplets of cross-links defining triangles of area $\sim r^2$ with shapes close to equilateral triangles. From nodal displacement of a triangle, the normal strains along its sides are first computed. Then the entire strain tensor over the area covered by the triangular domain is obtained from these normal strains. This local strain tensor denotes the average strain tensor of the underlying discrete deformation field over a length scale r proportional to the square root of the area of the respective triangle. In order to carry out the required averaging in Eq. (3), a large number of triangles is defined by randomly selecting three random cross-links, and the strain tensors are binned and averaged according to the size of the triangles.

The following parameters define the overall mechanical behavior of fiber networks. The structure of a network is represented by the normalized fiber density ρ, which is defined as the total length of the filaments multiplied by R divided by the area of the simulation domain. Since the orientation of individual fibers has uniform distribution, ρ fully defines their microstructure. In this work, the fiber density is varied from 0.005 to 0.05. Furthermore, the parameter l_b is assumed to be 5×10^{-5} unless otherwise mentioned. Finally, based on our previous results [16], the system size W is taken large in order to minimize finite-size effects. Nevertheless, no finite-size analysis is done in this work. Thus the findings, especially for dense networks, may involve some size effects; smaller simulation domains are used for dense systems because of the computational time constraint [27].

III. RESULTS

In Fig. 2, the length-scale-dependent nonaffinity measure is used to characterize the nonaffine behavior of type I fiber networks with $\rho \sim 0.01$, subjected to the uniform uniaxial strain field. It is observed that all three components of the nonaffinity measure are length scale dependent i.e., as the scale of observation becomes smaller, the amount of nonaffinity increases. Furthermore, the nonaffinity measure components follow a power-law scaling with the probing length scale. The scaling exponent is 1.74 ± 0.08. The results shown in Fig. 1 are very similar to previous studies on Mikado fiber networks

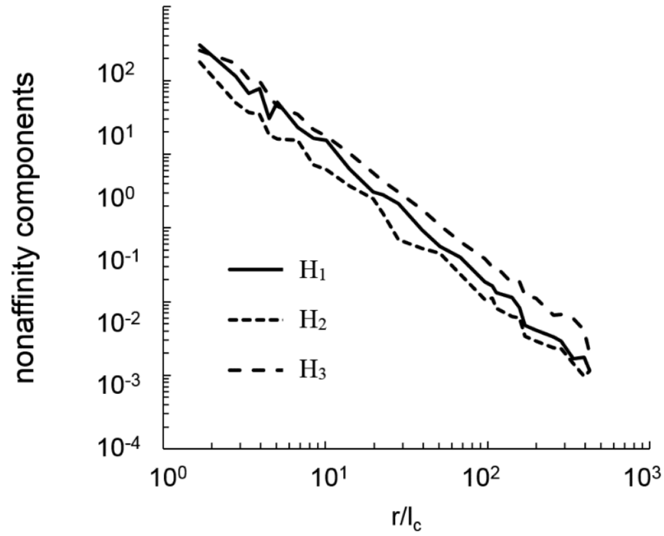

FIG. 2. The components of the strain-based nonaffinity measure, Eq. (3), as a function of normalized probing length scale for a type I fiber network with a fiber density $\rho = 0.01$ and when it is subjected to a uniaxial strain.

(type II networks) [16]. In particular, although nonaffinity decreases with increasing probing length scale, it is always nonzero. Thus, the deformation of type I networks, similar to that of type II networks, is always nonaffine and there exists no characteristic length scale separating affine and nonaffine deformation.

The effect of fiber density on nonaffine response of both fiber network types is shown in Fig. 3 by plotting the scalar nonaffinity measure defined in Eq. (2). For both types of fiber networks, the nonaffinity becomes more pronounced as the fiber density decreases. This agrees with previous work on type II networks [14–16]. Figure 3 shows that, at constant fiber density, type I networks deform more affinely than type II

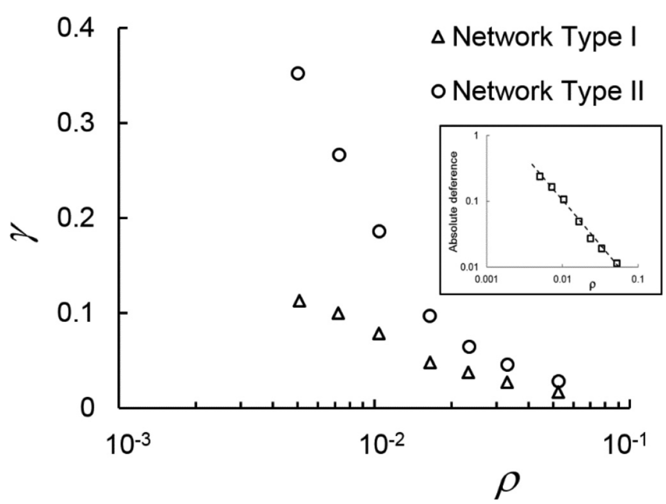

FIG. 3. The variation of the scalar nonaffinity measure γ as a function of fiber density for both network types. The nonaffinity measure of type II networks is always larger than that of type I networks. Furthermore, the absolute nonaffinity difference is inversely proportional to the fiber density (inset).

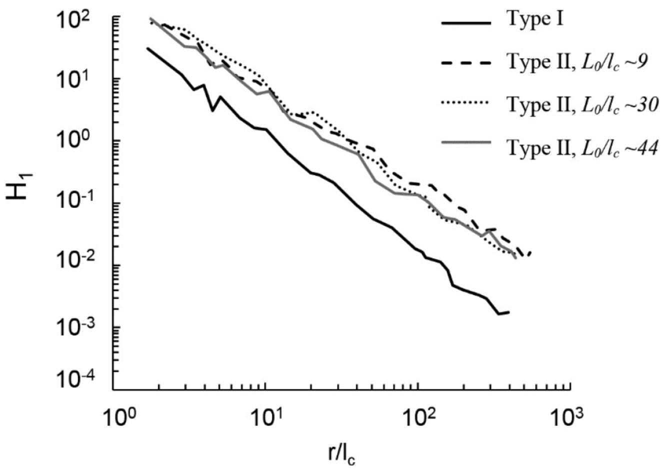

FIG. 4. The first component of the strain-based nonaffinity measure H_1 as a function of normalized probing length scale for type I and type II networks with fiber density of 0.01. At a given fiber density, L_0/W affects the architecture of type II networks by changing the values of L_0/l_c.

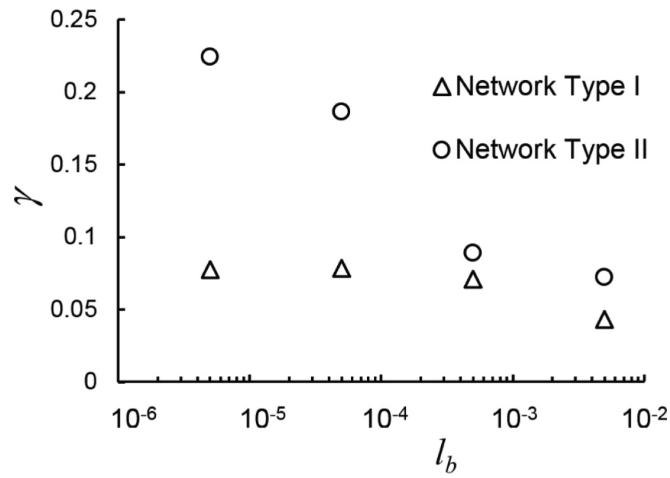

FIG. 5. The variation of the scalar nonaffinity measure γ as a function of parameter l_b (filament flexibility) for both network types. The nonaffinity measure of type II (Mikado) networks is always larger than that of type I networks.

networks. However, the absolute difference between the two decreases with increasing the fiber density following a power law with the exponent of about 1.4.

In order to investigate possible differences between two network types, we create Mikado fiber networks with similar fiber density as type I networks shown in Fig. 2. Figure 4 compares the first component of the length-scale-dependent nonaffinity measure in these two types of networks (the other nonaffinity components behave similarly). This figure shows that, at the constant normalized fiber density, the behavior of Mikado networks is more nonaffine compared to the behavior of type I networks. Both network types at each fiber density have similar parameter l_b and segment length distribution. Furthermore, the average orientation of their fibers as measured by the orientation tensor is similar. The orientation tensor is given by

$$\Omega = \frac{1}{\sum_i l_i} \sum_i l_i \begin{pmatrix} {c_i}^2 & c_i s_i \\ s_i c_i & {s_i}^2 \end{pmatrix}, \tag{4}$$

where c_i and s_i are the cosine and sine of the angle that a filament with length l_i makes with a reference axis. It is seen that $\Omega_{11} \sim \Omega_{22} \sim 0.5$ and $\Omega_{12} \sim 0$; i.e., both type I and II networks are isotropic. Thus the connectivity of the structures (characterized by coordination number) and relative arrangement of the fibers (measured by fiber density distribution) could be why their behavior is different.

Type I networks considered in the present study form a connected network independent of their fiber density. Nevertheless, fibers in type II (Mikado) networks form disconnected small clusters of filaments when the fiber density is low. With increasing fiber density, these clusters join together and a percolated network is formed. It is known that these networks acquire geometric percolation at a critical fiber density, which is proportional to $L_0/l_c \sim 6$. Note that l_c is mean segment length and is proportional to fiber density [15,28]. Previous work has shown that the mechanical response of Mikado networks, which are created using a constant initial fiber length L_0, is a function of l_c. At a given fiber density and depending on the values of L_0/W, type II networks with different values of L_0/l_c can be obtained. In order to ensure that the observation in Fig. 4 is not an artifact of the variation in L_0/l_c, we create Mikado networks with different $L_0/l_c \sim 9$, 30, and 44 while keeping the fiber density constant in all of them. These networks show almost similar response and their deformation is more nonaffine than that of type I networks. These Mikado fiber networks behave similarly because at low values of l_b, the fiber continuity is lost and individual fiber segments of a filament deform independently from each other. However, it is noted that the behavior of these networks will become a function of L_0/l_c with increasing l_b as discussed in previous studies [15,16].

The effect of fiber flexibility (parameter l_b) on the scalar nonaffinity measure for both types of network at a fiber density of 0.01 is shown in Fig. 5. As the ratio of bending stiffness and stretching stiffness of the filaments increases, their behavior becomes more affine in both network types. Furthermore, the behavior of type II networks (Mikado networks) is more nonaffine compared to the response of type I fiber networks.

The connectivity of the fibers in these two network types is different from each other. In type II networks, because most likely two fibers will cross at the any cross-link, the coordination number is 4. As stated before, dangling ends are formed in Mikado networks, which will be removed in numerical simulations since they do not contribute to the total energy of the system. The omission of these dangling ends reduces slightly the overall coordination of type II networks. However, the coordination number of type I networks at all cross-links is 3. Considering the critical Maxwell coordination number (connectivity) for two-dimensional central-force networks, type II networks are close to the isostatic point ($z = 4$) while type I networks are well below ($z = 3$). Thus, the finite bending stiffness of filaments and rigid cross-links between these filaments are required to ensure the stability of both network types.

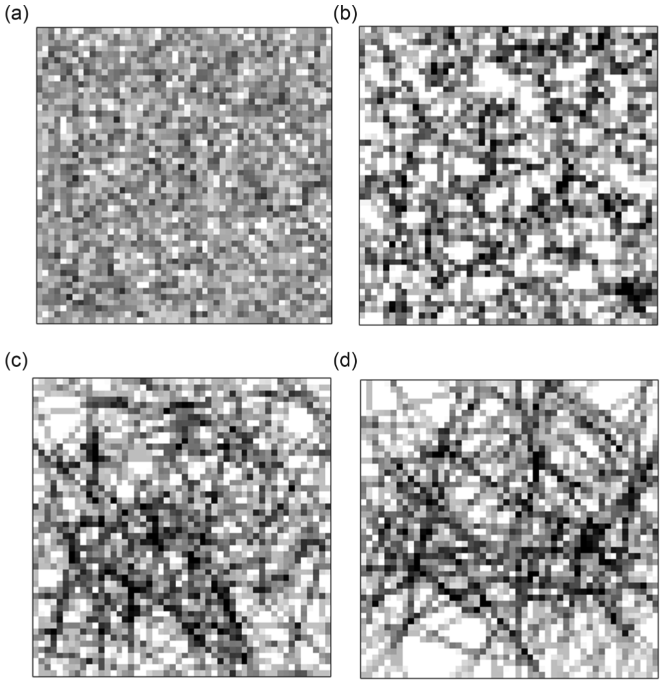

FIG. 6. Comparison of fiber density distribution maps: (a) Type I networks, (b) type II networks with $L_0/l_c \sim 9$, (c) type II networks with $L_0/l_c \sim 30$, and (d) type II networks with $L_0/l_c \sim 44$. It is seen that fiber networks generated by growing straight lines from seed points have a more uniform density distribution compared with those generated using the Mikado algorithm.

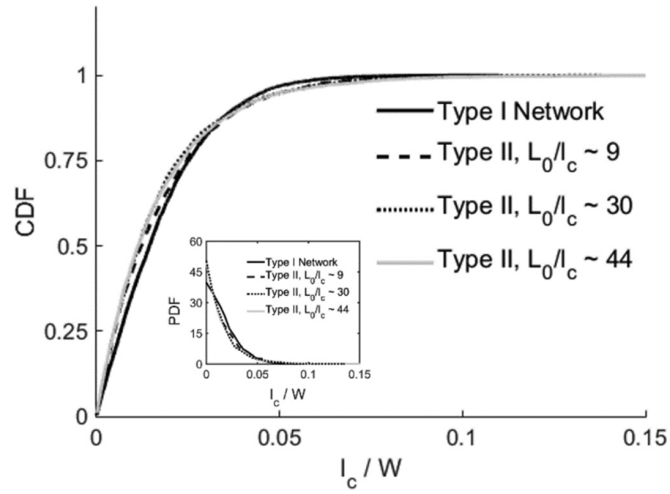

FIG. 7. The cumulative probability distribution (CDF) and probability distribution (PDF) of fiber segments for networks shown in Fig. 6. This plot confirms that both network generation algorithms at similar fiber density yield random fiber networks with almost the same segment length probability distribution function. Thus, the difference in the deformation of these networks should be because of spatial distribution of fiber segments.

It is well-documented that with decrease of isostaticity, the behavior of fiber networks becomes bending dominated and subsequently more nonaffine. With regard of this statement, the results shown in Figs. 4 and 5 seem counterintuitive. In other words, it is expected that the nonaffinity is more pronounced in type I networks since they have a lower connectivity. In order to further investigate the origin of this significant difference in the behavior of these two network types, we characterize the distribution of fibers inside the domain. For this purpose, we discretize the networks by overlaying a regular grid of square elements. In each square of the grid, we calculate the total length of fibers and divide it by the total length of fibers inside the simulation box. This grid will yield a map of fiber length distribution which is plotted in Fig. 6.

In Fig. 7, we plot the fiber segment distribution. It is seen that although both network types have almost the same segment length distribution, their relative arrangements are very different from each other. The spatial distribution of fibers in type I networks is more uniform compared to that of Mikado fiber networks. The uniformity of fiber density distribution in networks grown from random seeds allows them to distribute the load more evenly between filaments and subsequently create a more homgenous structure in response to the applied far-field load. On the other hand, the Mikado networks depict large peaks of density which are connected together by individual filaments. This feature causes large rotation and deformation in type II networks and will subsequently render their elastic field to be more nonaffine.

Based on the above discussion, it is expected that most of the filaments in type I networks contribute mechanically to resist the external deformation. In order to check this assumption, we obtain the energy distribution inside the networks by using the same square grid. Here, the total energy of the fibers that are inside a square are summed together and divided by the total energy of the system. Clear force chains appear in both types of networks, Fig. 8. Nevertheless, the nature of force chains is very different from each other. This further emphasizes the significant role of network microstructure on the mechanical response of random fiber networks.

At this point, a note should be made about the relevance of investigating the behavior of fibrous materials using 2D network models. Real biological materials such as cytoskeleton and extracellular matrix are three dimensional. However, because 2D simulations, compared to three-dimensional models, are much less computationally intensive, 2D models have been widely used for investigating the mechanical behavior of these structures [14–19]. In real three-dimensional (3D) fiber networks, filaments do not generally intersect with each other and are connected together with cross-links. Thus, the density and mechanical properties of both the filaments and the cross-links are required in numerical models. Previous studies have shown that despite inevitable differences between 2D and 3D network models, there exist certain similarities. For example, the mean filament segment length is inversely proportional to the total fiber length density in both 2D and 3D [3]. Based on previous studies, we can state that 2D fiber network models are useful tools for gaining a general idea about the behavior of real 3D networks. For instance, in a recent study, we extended the Mikado model to 3D in order to characterize the differences and similarities between the mechanical behavior of 2D and 3D network models [29,30]. We found that the

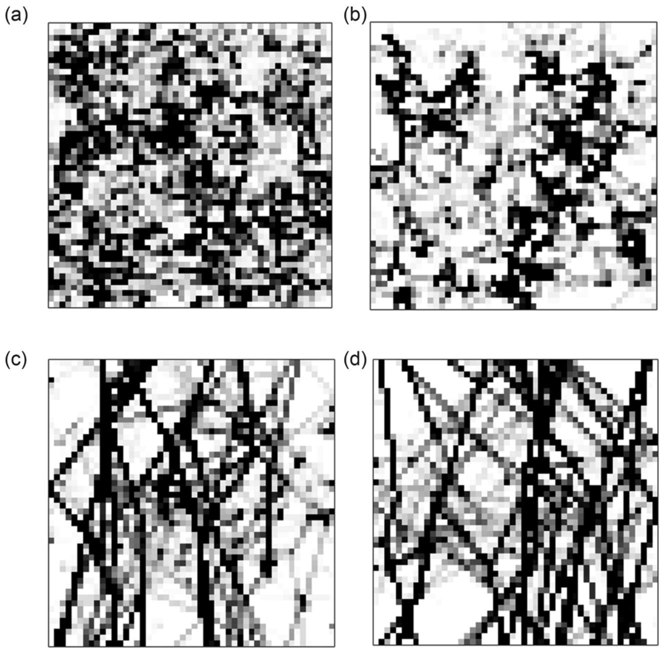

FIG. 8. Comparison of total filament energy distribution maps: (a) Type I networks, (b) type II networks with $L_0/l_c \sim 9$, (c) type II networks with $L_0/l_c \sim 30$, and (d) type II networks with $L_0/l_c \sim 44$. It is seen that fiber networks generated by growing straight lines from seed points have a more uniform energy distribution compared with those generated using the Mikado algorithm.

degree of nonaffinity has a power-law dependence on probing length scale in both models. Furthermore, we observed that the amount of nonaffinity increases with decreasing filament bending stiffness and fiber density in both 2D and 3D networks. Nevertheless, the degree of nonaffinity was found to be more significant in 3D than in 2D networks. Future studies are required to determine the capability of 2D growing networks, studied here, in representing the behavior of real 3D networks. Until then, the findings of the present study should be treated with caution and only as an approximation for the actual complex behavior of 3D biomaterials.

In conclusion, it is observed that fiber networks which are grown from random seed points similar to Mikado fiber networks at all probing length scales show nonaffine mechanical behavior and their nonaffinity varies as a power law. The nonaffinity is a function of fiber density and flexibility of constituting filaments. Nevertheless, despite a lower coordination number, the nonaffinity in these networks is smaller than the nonaffinity of Mikado networks at similar fiber density. The numerical model developed here shows that Mikado networks have less uniform distribution of fiber density and total energy. This inherent dispersity results in more significant nonaffinity.

ACKNOWLEDGMENTS

The author would like to acknowledge the support in part by National Science Foundation under Grant No. 1351461.

[1] C. P. Broedersz and F. C. MacKintosh, Modeling semiflexible polymer networks, Rev. Mod. Phys. **86**, 995 (2014).
[2] H. Hatami-Marbini and C. R. Picu, Modeling the mechanics of semiflexible biopolymer networks: non-affine deformation and presence of long-range correlations, in *Advances in Soft Matter Mechanics*, edited by S. Li and B. Sun (Springer, Heidelberg, 2012), pp. 119–145.
[3] R. Picu, Mechanics of random fiber networks—a review, Soft Matter **7**, 6768 (2011).
[4] A. Kabla and L. Mahadevan, Nonlinear mechanics of soft fibrous networks, J. R. Soc., Interface **4**, 99 (2007).
[5] L. J. Gibson and M. F. Ashby, *Cellular Solids: Structure and Properties* (Cambridge University Press, Cambridge, 1997).
[6] H. Hatami-Marbini and M. R. Mofrad, Rheology and mechanics of the cytoskeleton, in *Complex Fluids in Biological Systems*, edited by S. Spagnolie (Springer, New York, 2015), pp. 187–205.
[7] H. Hatami-Marbini and M. R. Mofrad, Cytoskeletal mechanics and cellular mechanotransduction: a molecular perspective, in *Cellular and Biomolecular Mechanics and Mechanobiology*, edited by A. Gefen (Springer-Verlag, Heidelberg, 2011), pp. 3–27.
[8] B. Alberts, A. Johnson, J. Lewis, M. Raff, K. Roberts, and P. Walter, *Molecular Biology of the Cell* (Garland Science, New York, 1994).
[9] M. L. Gardel, J. H. Shin, F. C. MacKintosh, L. Mahadevan, P. Matsudaira, and D. A. Weitz, Elastic behavior of cross-linked and bundled actin networks, Science **304**, 1301 (2004).
[10] P. A. Janmey, M. E. McCormick, S. Rammensee, J. L. Leight, P. C. Georges, and F. C. MacKintosh, Negative normal stress in semiflexible biopolymer gels, Nat. Mater. **6**, 48 (2007).
[11] C. Storm, J. J. Pastore, F. C. MacKintosh, T. C. Lubensky, and P. A. Janmey, Nonlinear elasticity in biological gels, Nature **435**, 191 (2005).
[12] M. Rubinstein and R. H. Colby, *Polymer Physics* (Oxford University Press, New York, 2003), Vol. 23.
[13] D. Rodney, M. Fivel, and R. Dendievel, Discrete Modeling of the Mechanics of Entangled Materials, Phys. Rev. Lett. **95**, 108004 (2005).
[14] J. Wilhelm and E. Frey, Elasticity of Stiff Polymer Networks, Phys. Rev. Lett. **91**, 108103 (2003).
[15] D. A. Head, A. J. Levine, and F. C. MacKintosh, Distinct regimes of elastic response and deformation modes of cross-linked cytoskeletal and semiflexible polymer networks, Phys. Rev. E **68**, 061907 (2003).
[16] H. Hatami-Marbini and R. C. Picu, Scaling of nonaffine deformation in random semiflexible fiber networks, Phys. Rev. E **77**, 062103 (2008).
[17] H. Hatami-Marbini and R. Picu, Effect of fiber orientation on the non-affine deformation of random fiber networks, Acta Mech. **205**, 77 (2009).
[18] P. Onck, T. Koeman, T. van Dillen, and E. van der Giessen, Alternative Explanation of Stiffening in Cross-Linked Semiflexible Networks, Phys. Rev. Lett. **95**, 178102 (2005).
[19] H. Hatami-Marbini and R. C. Picu, Heterogeneous long-range correlated deformation of semiflexible random fiber networks, Phys. Rev. E **80**, 046703 (2009).

[20] B. A. DiDonna and T. C. Lubensky, Nonaffine correlations in random elastic media, Phys. Rev. E **72**, 066619 (2005).
[21] S. A. Langer and A. J. Liu, Effect of random packing on stress relaxation in foam, J. Phys. Chem. B **101**, 8667 (1997).
[22] A. Tanguy, J. P. Wittmer, F. Leonforte, and J. L. Barrat, Continuum limit of amorphous elastic bodies: A finite-size study of low-frequency harmonic vibrations, Phys. Rev. B **66**, 174205 (2002).
[23] C. P. Broedersz, M. Sheinman, and F. C. MacKintosh, Filament-Length-Controlled Elasticity in 3D Fiber Networks, Phys. Rev. Lett. **108**, 078102 (2012).
[24] P. L. Chandran and V. H. Barocas, Affine versus non-affine fibril kinematics in collagen networks: Theoretical studies of network behavior, J. Biomech. Eng. **128**, 259 (2006).
[25] K. E. Kadler, D. F. Holmes, J. A. Trotter, and J. A. Chapman, Collagen fibril formation, Biochem. J. **316**, 1 (1996).
[26] A. O. Brightman, B. P. Rajwa, J. E. Sturgis, M. E. McCallister, J. P. Robinson, and S. L. Voytik-Harbin, Time-lapse confocal reflection microscopy of collagen fibrillogenesis and extracellular matrix assembly in vitro, Biopolymers **54**, 222 (2000).
[27] A. Shahsavari and R. C. Picu, Model selection for athermal cross-linked fiber networks, Phys. Rev. E **86**, 011923 (2012).
[28] J. A. Åström, J. P. Mäkinen, M. J. Alava, and J. Timonen, Elasticity of Poissonian fiber networks, Phys. Rev. E **61**, 5550 (2000).
[29] H. Hatami-Marbini, Nonaffine behavior of three-dimensional semiflexible polymer networks, Phys. Rev. E **93**, 042503 (2016).
[30] H. Hatami-Marbini, Scaling properties of three-dimensional random fibre networks, Philos. Mag. Lett. **96**, 165 (2016).